

Ultrathin g-C₃N₄/TiO₂ composites as photoelectrochemical elements for real-time evaluating of global antioxidant capacity

Weiguang Ma^{a,b}, Dongxue Han^{a,b}, Min Zhou^{a,b}, Hao Sun^c, Lingnan Wang^{a,b}, Xiandui Dong^{a,b} and Li Niu^{a,b*}*

a State Key Laboratory of Electroanalytical Chemistry, c/o Engineering Laboratory for Modern Analytical Techniques,

Changchun Institute of Applied Chemistry, Chinese Academy of Sciences

Changchun, Jilin 130022 (P. R. China)

b Graduate University of Chinese Academy of Sciences, Chinese Academy of Sciences,

Beijing 100039 (P. R. China)

c College of chemistry, Northeast Normal University

Changchun, Jilin 130022(P. R. China)

Experimental Section

Chemical reagents

Titanium trichloride (TiCl_3), Terephthalic acid (TA), Gallic acid (GA), Rutin trihydrate (RT), Quercetin dehydrate (QR), and 1,1-Diphenyl-2-picrylhydrazyl radical 2,2-Diphenyl-1-(2,4,6-trinitrophenyl) hydrazyl (DPPH) were obtained from Alfa. Ascorbic acid (AA), L-glutathione reduced (GSH), Caffeic acid (CA), Catechin hydrate (CT), Fisetin(FT), 6-Hydroxy-2,5,7,8-tetramethylchromane-2-2-carboxylic acid (Trolox), L-cysteine (Cys), Glucose, Melamine and Folin-Ciocalteu (F-C) reagent (10 %) were obtained from Sigma-Aldrich. Other reagents were used as received without purification. The PBS buffer was made from sodium phosphate ($\text{NaH}_2\text{PO}_4/\text{Na}_2\text{HPO}_4$, 81:19 (molar ratio)) and sodium chloride dissolved in deionized water at final concentrations of 10 mmol L^{-1} (pH: 7.4).

Characterization

X-ray diffraction (XRD) patterns of the samples were carried out in the range of $10\text{-}80^\circ$ (2θ) using a D/MAX 2500V/PC X-ray diffraction ($\text{Cu K}\alpha$ radiation, $\lambda = 0.15406 \text{ nm}$), operated at 40 kV and 30 mA. X-ray photoelectron spectroscopy (XPS) was recorded with an ESCALAB-MK II 250 photoelectron spectrometer with $\text{Al K}\alpha$ X-ray radiation as the X-ray source for excitation. Transmission electron microscope (TEM) and high-resolution transmission electron microscope operating (HRTEM) images were obtained with a TECNAI G2 high-resolution transmission electron microscope operating at 200 kV. Scanning electron microscope (SEM) images were recorded with a XL30 environmental scanning electron microscope (ESEM, Philips Electron Optics) with finite element model and 20 kV accelerating voltage. The UV-visible diffused reflectance spectra (DRS) were performed on the dry-pressed disk samples using a Hitachi U-3900 spectrophotometer equipped with an integrating sphere assembly, using BaSO_4 as the reference sample. Fluorescence emission spectra were recorded on a Hitachi F-4600 fluorescence spectrophotometer. Fourier transform infrared spectroscopy (FTIR) spectrum was recorded using a Bruker Tensor 27 Spectrometer. The thickness of ultrathin $\text{g-C}_3\text{N}_4$ nanosheets were checked by atomic force microscopy (AFM, Agilent AFM 5500 Agilent Technologies, Chandler, AZ) in tapping mode at room temperature. All electrochemical experiments were performed with a CHI660A Electrochemical Workstation(CHI) and a conventional three-electrode system, comprising ITO or modified ITO as working electrode, a platinum wire as the auxiliary electrode, and a Ag/AgCl electrode ($3 \text{ mol}\cdot\text{L}^{-1}$ KCl) as reference electrode. All the potentials were reported versus Ag/AgCl reference electrode at room temperature. The PBS solution was applied as supporting electrolyte and bubbled with N_2 for 15min before experiment. LED light (420 nm, Beijing Perfectlight Technology) was used as source of photoelectrochemical sensor. Peristaltic pump was purchased from longerpump (BT100-2J). Electrochemical impedance spectroscopy (EIS) measurements were performed using a Solartron 1255 B Frequency Response Analyzer (Solartron Inc.UK) in mixed solution of $5 \text{ mmol}\cdot\text{L}^{-1}$ $[\text{Fe}(\text{CN})_6]^{3-/4-}$ and $0.1 \text{ mol}\cdot\text{L}^{-1}$ KCl aqueous solution. Mott-Schottky plot was obtained in $1 \text{ mol}\cdot\text{L}^{-1}$ Na_2SO_4 with frequencies of 1000 and 2000 HZ.

Preparation of utg- $\text{C}_3\text{N}_4/\text{TiO}_2$ nanopaticles

Bulk $\text{g-C}_3\text{N}_4$ was first synthesized with thermal polycondensation of melanin in argon at 550°C with a heating rate of 2.5 K min^{-1} for 2h. The obtained bulk $\text{g-C}_3\text{N}_4$ was rinsed with water and ethanol three times, respectively, dried at 70°C . Then, 50mg bulk $\text{g-C}_3\text{N}_4$ was dispersed in 50 mL water and ultrasonic for 2h. The ultrathin $\text{g-C}_3\text{N}_4$ (utg- C_3N_4) was dispersed in supernatant, which was centrifuged at $3500 \text{ r}\cdot\text{min}^{-1}$ for 20min, and the supernatant was collected and prepared to be used. The utg- $\text{C}_3\text{N}_4/\text{TiO}_2$ composites were synthesized by using the self-assembly method. Typically, first 3 mL utg- C_3N_4 and 0.11 mL sodium dodecylsulfate (SDS, $0.05 \text{ mol}\cdot\text{L}^{-1}$) were added to 70.73 mL water, then 50mL TiCl_3 ($0.12 \text{ mol}\cdot\text{L}^{-1}$) was introduced with modest stirring for one hour. Subsequently 10 mL of Na_2SO_4 ($0.6 \text{ mol}\cdot\text{L}^{-1}$) and 5 mL of H_2O_2 (1 wt%) were added, and the obtained mixed solution was stirred for 16 hours at 90°C . Next, the separated precipitates were washed with water and ethanol for three times, dried at 70°C , and then calcined in nitrogen at 400°C with a heating rate of 2 K min^{-1} for 2h. Finally, the obtained

composites were treated with a cleaning process involving three cycles of centrifugation/ washing/ re-dispersion in water and dried at 70°C in air. The control experiments using bulk g-C₃N₄ or deionized water were also performed as described above.

The process of assay on photoelectrochemical sensor

The ITO electrode was first cleaned with NaOH (1 mol L⁻¹) and H₂O₂ (30%), then washed with acetone and twice-distilled water, and dried at room temperature. After that, 100 μL of the utg-C₃N₄/TiO₂ suspension (1 mg mL⁻¹) was cast onto the ITO electrode and dried at room temperature to obtain an utg-C₃N₄/TiO₂-modified ITO electrode. The bg-C₃N₄/TiO₂ and TiO₂ modified ITO electrode was prepared similarly. Cross-sectional view of the utg-C₃N₄/TiO₂ film was shown in Figure S1 and the film was found to be about 400nm.

As shown in figure S6c, first, the thin layer photoelectrochemical flow cell was fixed. Then, the buffer or sample was injected into the flow cell with Peristaltic pump at 2 r•min⁻¹. The light irritated from the back side of the work electrode (an illumination power on the work electrode of 73.89 mW/cm²), which can efficiently prevent the interference from the color sample. Every sample was detected for three times and the average value was calculated. The photoelectrocurrent was collected according to the following rule: $I = I_{\text{sample}} - I_{\text{blank}}$ (I_{sample} , the photoelectrochemical current of the sample, I_{blank} , the photoelectrochemical current without sample).

Four brands of tea and four brands of coffee were obtained from local supermarket without pretreatment before detection. 0.5 g tea was added into 50 mL boiling deionized water, and then it was filtered by normal funnel after 30 min extraction. 0.25 g coffee was added into 25mL boiling deionized water, and then filtered by normal funnel after 3 min extraction. Both the filtrate were diluted with PBS and used for further antioxidant capacity determination.

The detection of antioxidant capacity with reference methods

Folin-Ciocalteu (F-C) method was referenced by Ainsworth [1]. 100 μL of GA solution or various tea diluted solutions was added into 2-mL microtubers; then, 200 μL of F-C reagent (10%, v/v, Sigma) was introduced with a thorough vortex; at last, 800 μL of Na₂CO₃ (0.7 mol•L⁻¹) was added to the above solution and the mixture was incubated at 20°C for 2 hours. The reacted system was detected by UV-visible spectrophotometer and the absorbance was recorded at 765nm.

DPPH radical scavenging activity was performed according to report of Brandwilliams et al with a little modification [2]. 5 mg DPPH was dissolved in 125 mL absolute methanol. 0.2 mL Trolox solution or various of tea diluted sample solutions was added into 0.8 mL DPPH solution and reacted for 15 min without light. The reacted solution was immediately detected by UV-visible spectrophotometer and the absorbance was recorded at 514 nm.

Calculation of Ionization potential (IP) values

Gas-phase adiabatic ionization potential (IP) of all the compounds were calculated at 298 K using B3LYP[3] method combined with the 6-311G(d, p) basis set[4]. All computations were performed by Gaussian 09 program[5].

Results

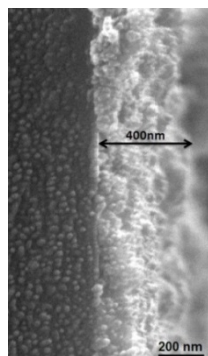


Figure S1. Cross-sectional view of the utg-C₃N₄/TiO₂ film.

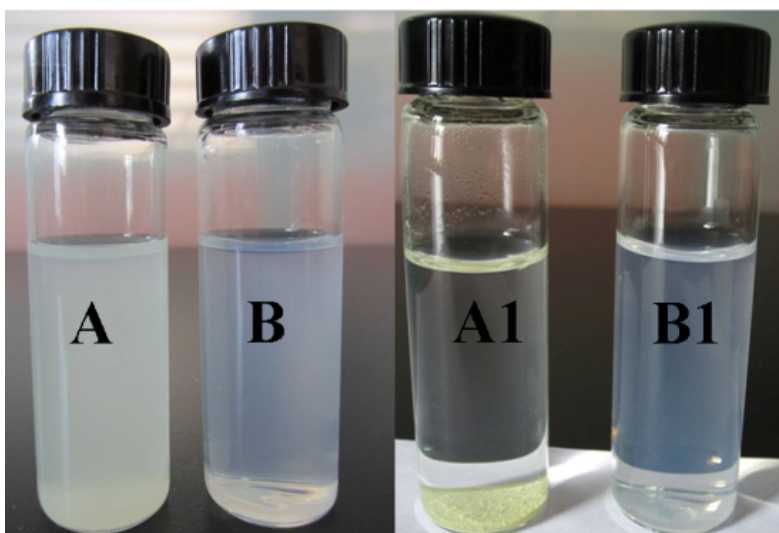


Figure S2. The digital images of bulk-g-C₃N₄ (A, A₁) and utg-C₃N₄ (B, B₁). A₁ and B₁ are the same samples recorded two weeks later.

Compared to bulk-g-C₃N₄, the utg-C₃N₄ demonstrated uniform dispersion in water even after two weeks. However, obvious precipitate can be found in bulk-g-C₃N₄ suspension soon. It revealed that ultrasonic method played a significant role in improvement of the poor solubility of g-C₃N₄.

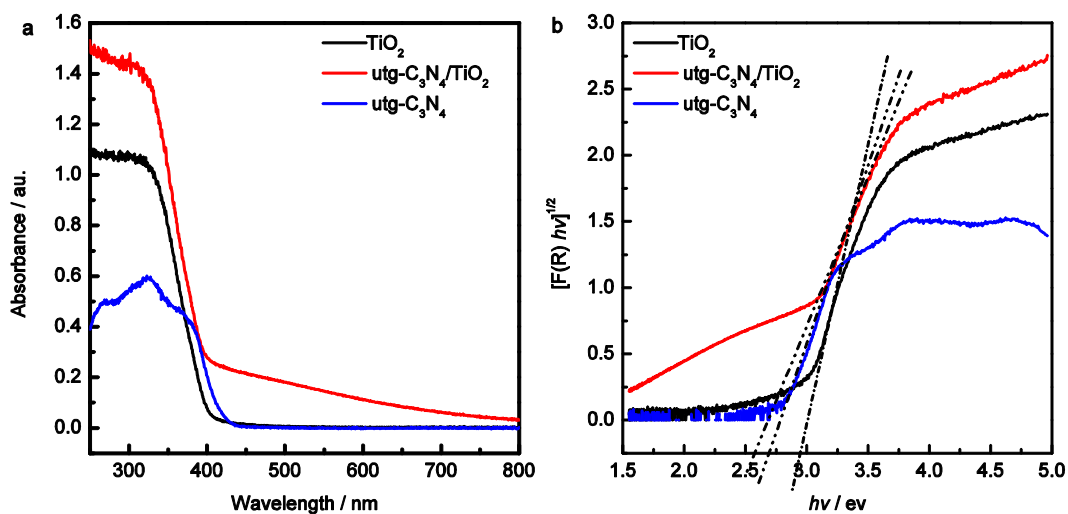


Figure S3. The UV-vis DRS (a) and the plot of transformed Kubelka-Munk function versus the energy of light (b) for TiO₂ (black), utg-C₃N₄ (blue) and utg-C₃N₄/TiO₂ (red).

UV-vis diffuse reflectance spectra (DRS) of TiO₂, utg-C₃N₄ and utg-C₃N₄/TiO₂ have been recorded in Figure S3 (a). As can be seen clearly that compared to the pristine TiO₂, the introducing of utg-C₃N₄ induces the increased light absorption intensity in both of the UV and visible light regions. The width of the band gap of the photocatalyst was a key role to determine the light absorption. A plot of the transformed Kubelka-Munk function as a function of energy of light is shown in Figure S3 (b), by which the roughly estimated band gaps are 2.98, 2.70 and 2.58 eV corresponding to TiO₂, utg-C₃N₄ and utg-C₃N₄/TiO₂ respectively. Due to the distinct band gap narrowing of TiO₂, the photoelectrochemical property under visible light regions can be effectively improved.

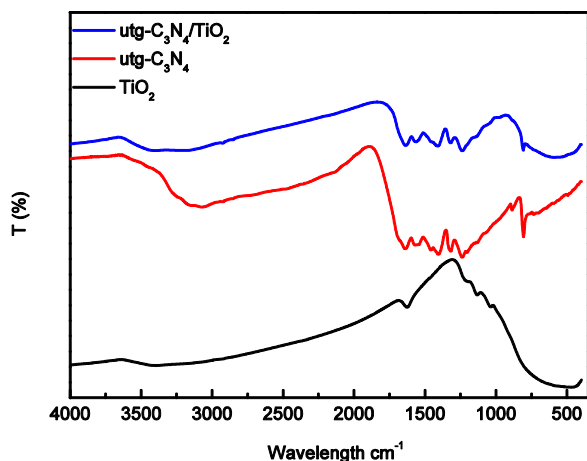


Figure S4. FTIR spectra of TiO_2 (black), $\text{utg-C}_3\text{N}_4$ (red) and $\text{utg-C}_3\text{N}_4/\text{TiO}_2$ (blue).

As shown in Figure S4 (red), the broad peaks between 3500 and 3000 cm^{-1} originating from the N–H stretches can be clearly observed, suggesting the partial hydrogenation of some nitrogen atoms in the nanosheets. The peak at 2150 cm^{-1} is attributed to cyano terminal groups $\text{C}\equiv\text{N}$, and the set of peaks between ~ 1700 and 900 cm^{-1} is characteristic of s-triazine derivatives [6]. These specific peaks were also observed on the spectra of $\text{utg-C}_3\text{N}_4/\text{TiO}_2$, which is also in present of specific peaks of TiO_2 (low 1000 cm^{-1}) [7]. Therefore, the results of FTIR further proved that $\text{utg-C}_3\text{N}_4/\text{TiO}_2$ was successfully synthesized.

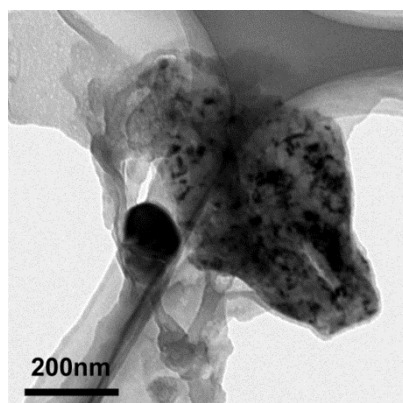


Figure S5. TEM image of bulk $\text{g-C}_3\text{N}_4/\text{TiO}_2$.

Compared with $\text{utg-C}_3\text{N}_4$, TiO_2 nanoparticles can hardly disperse on the surface of bulk $\text{g-C}_3\text{N}_4$ (shown in Figure S5) due to its poor solubility. It might be one of the reasons for which $\text{g-C}_3\text{N}_4/\text{TiO}_2$ present more excellent photoelectrochemical prosperity than that of bulk $\text{g-C}_3\text{N}_4/\text{TiO}_2$.

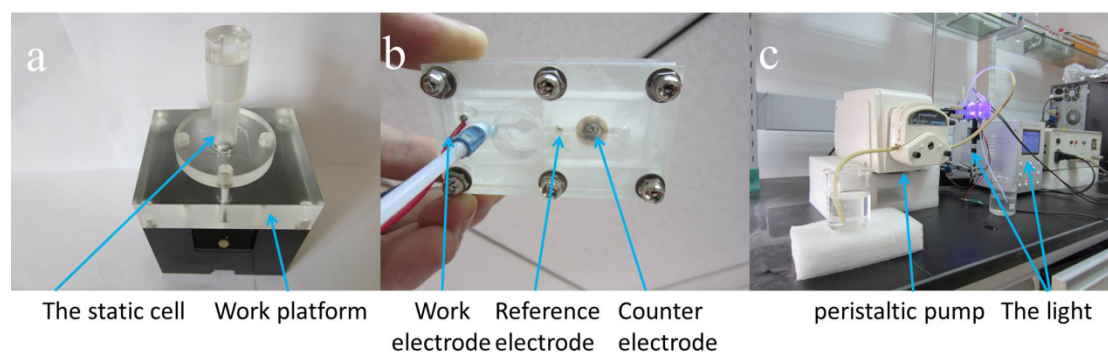


Figure S6. The image of the static cell (a), thin layer photoelectrochemical sensor (b) and the whole detection instrument of thin layer photoelectrochemical sensor (c).

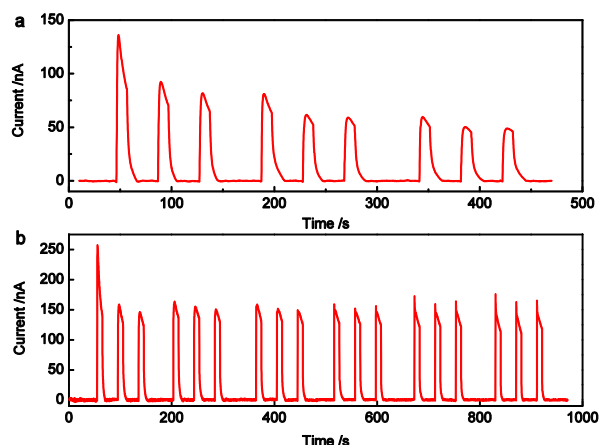


Figure S7. The photocurrent of static cell (a) and flow cell (b) in $0.1 \text{ mol}\cdot\text{L}^{-1}$ PBS containing $20 \text{ }\mu\text{mol}\cdot\text{L}^{-1}$ GA at 0 V under 420 nm light excitation.

As shown in figure S7a, the photocurrent decreased with increase of the assay times, since the reaction product should be absorbed on the modified electrode and then affects the following detection. However, when the flow cell was applied, the reaction product could flow out and not further poison the modified electrode. Therefore, the photocurrent almost has no influence on the assay time (figure S7b).

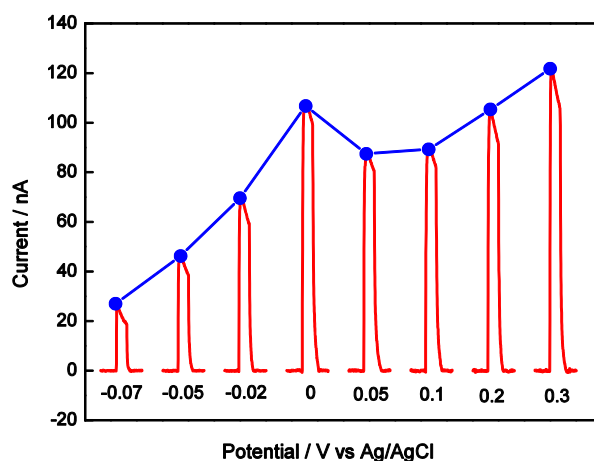


Figure S8. Effects of applied potential on photocurrent response of $\text{utg-C}_3\text{N}_4/\text{TiO}_2$ modified ITO in $0.1 \text{ mol}\cdot\text{L}^{-1}$ PBS (pH: 7.4) containing $10 \text{ }\mu\text{mol}\cdot\text{L}^{-1}$ GA under 420nm light excitation.

As shown in Figure S8, the photocurrent increment sharply increased as the applied potential increased from -0.07 V to 0 V and then seemed to be steady from 0V to 0.3V. The positive potential could drive electron from the CB of TiO_2 to ITO electrode, even when there was a relatively high concentration of electrons in the contact between ITO electrode and photocatalyst. The higher the applied potential used, the lower the electron concentration in the contact became, and the larger was the gradient near it. Therefore, the photocurrent became much higher. However, when the applied potential was more than 0 V, the electron concentration in the contact was negligible and the photocurrent no longer depends on potential. Therefore, 0 V was chosen to detect antioxidant capacity of antioxidants.

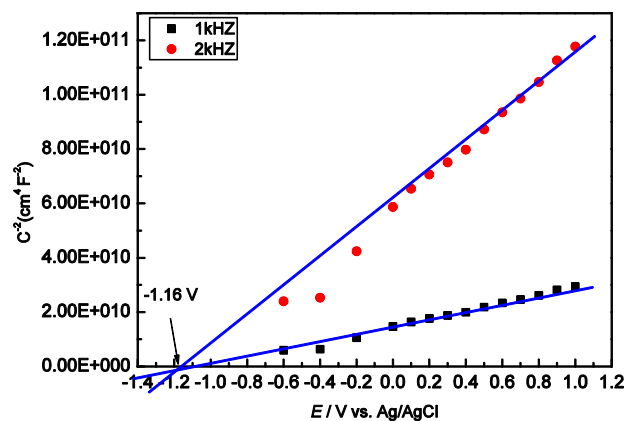


Figure S9. Mott-Schottky plot of utg-C₃N₄ in 1 mol·L⁻¹ Na₂SO₄ with frequencies of 1000 and 2000 Hz from -0.6 to 1.2 V.

Apparently, the Mott-Schottky plots of utg-C₃N₄ nanosheets under various frequencies disclose the typical n-type characteristic of organic semiconductors owing to the positive slope of the linear plots. More importantly, the derived flat band potential for utg-C₃N₄ nanosheets is about -1.16 V versus Ag/AgCl, which is smaller than that of bulk g-C₃N₄ [6].

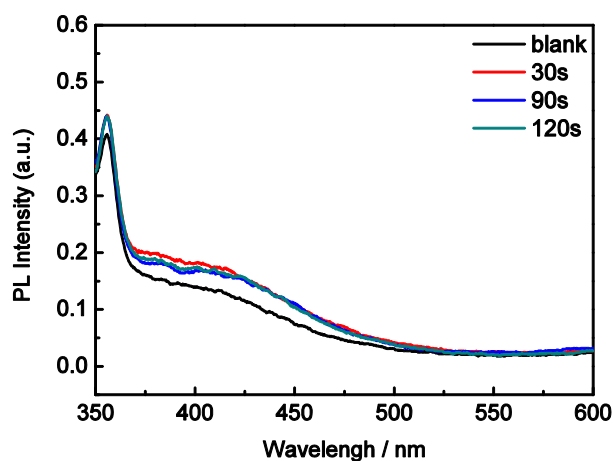


Figure S10. Fluorescence emission of 0.5 mmol·L⁻¹ terephthalic acid in PBS with light of 0, 30, 90 and 120 s min at excitation 315 nm.

With the increase of irradiation time, the specific peak (425 nm) was not observed; it demonstrated that hydroxyl radicals were not produced. It is the hole instead of the hydroxyl radicals that oxidized the antioxidants in the presented photoelectrochemical sensor.

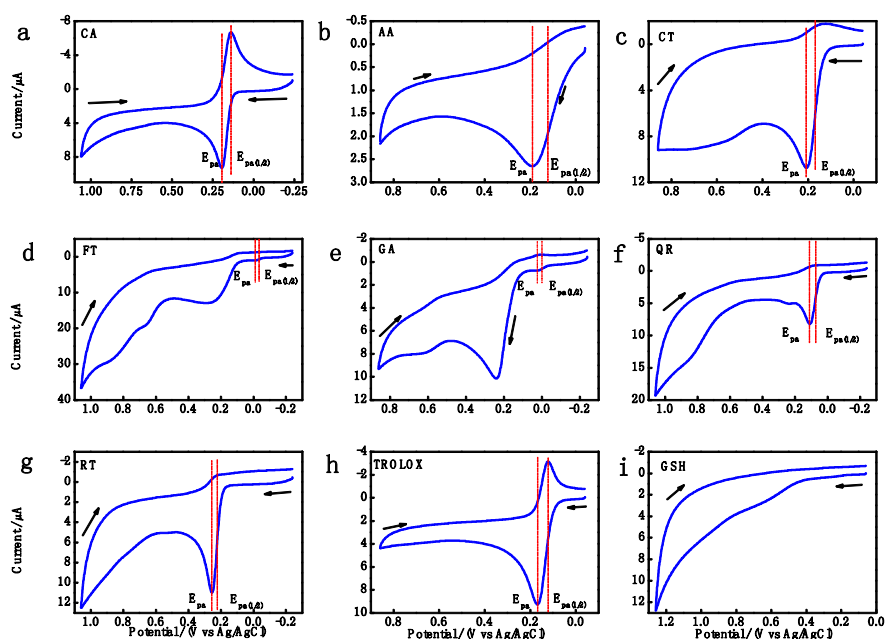


Figure S11. The CVs of $0.5 \text{ mmol}\cdot\text{L}^{-1}$ of nine antioxidants in $0.1 \text{ mol}\cdot\text{L}^{-1}$ PBS. The scan rate is $100 \text{ mV}\cdot\text{s}^{-1}$.

Since no return cathodic peak of several antioxidant molecules, the oxidative potential of antioxidants was expressed by the potential halfway between $E_{p/2}$ and E_{pa} of the first peak [8] in the present article. (E_{pa} , the potential of anodic peak; $E_{p/2}$, the half potential of anodic peak from the cathodic direction). The result can refer to the main article.

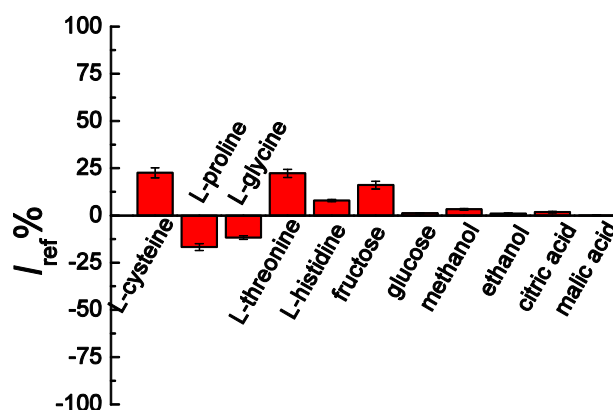


Figure S12. Photocurrent response of $\text{utg-C}_3\text{N}_4 / \text{TiO}_2$ modified ITO electrode upon addition of $25 \text{ mmol}\cdot\text{L}^{-1}$ each of L-proline, L-glycine, L-histidine, ethanol, methanol, $12.5 \text{ mmol}\cdot\text{L}^{-1}$ each of L-threonine, fructose, glucose, L-citric acid, L-malic acid, $0.5 \text{ mmol}\cdot\text{L}^{-1}$ L-cysteine in $0.1 \text{ mol}\cdot\text{L}^{-1}$ PBS (pH=7.4) contained $25 \mu\text{mol}\cdot\text{L}^{-1}$ GA at 0 V under 420 nm light excitation.

Table S1. Linear Equations, Correlation Coefficients (r^2), Redox Potential (E), Ionization potential, Antioxidant Capacity^a and Linear Ranges for Antioxidants.

Antioxidants	Linear equation	Linearity range ($\mu\text{mol L}^{-1}$)	R^2	E (V)	IP(kal mol^{-1})	Antioxidant capacity
Quercetin	$y = 3.150x - 14.62$	9.90~111.10	0.992	0.300	161.89	3.150
Gallic acid	$y = 3.17x + 12.21$	5.00~74.44	0.956	0.217	179.65	3.170
Caffeic acid	$y = 4.099x - 40.04$	15.00~193.31	0.993	0.374	175.72	4.099

Catechin	$y = 5.195x - 79.82$	24.96~192.31	0.992	0.394	166.27	5.195
Fisetin	$y = 3.375x - 89.35$	29.56~181.82	0.983	0.189	266.27	3.375
Rutin	$y = 1.571x + 14.175$	24.88~192.31	0.973	0.447	165.12	1.571
Trolox	$y = 0.117x + 25.31$	73.85~348.84	0.997	0.356	-6.73	0.117
Ascorbic acid	$y = 0.629x + 46.28$	25.00~243.09	0.970	0.365	182.64	0.629
Glutathione	$y = 0.039x + 8.824$	9.65~400.00	0.996	---	179.64	0.039

a: Antioxidant Capacity is obtained from the slope of standard calibration curve of each antioxidant compound^[9]. '---' means not obvious.

References

- [1] E. A. Ainsworth, K. M. Gillespie, *Nat. Protoc.* **2007**, *2*, 875-877.
- [2] W. Brandwilliams, M. E. Cuvelier, C. Berset, *Food Sci. Technol-leb* **1995**, *28*, 25-30.
- [3] a) A. D. Becke, *J. Chem. Phys.* **1993**, *98*, 5648-5652; b) A. D. Becke, *J. Chem. Phys.* **1992**, *96*, 2155-2160; c) C. T. Lee, W. T. Yang, R. G. Parr, *Phys. Rev. B* **1988**, *37*, 785-789.
- [4] a) A. D. McLean, G. S. Chandler, *J. Chem. Phys.* **1980**, *72*, 5639-5648; b) R. Krishnan, J. S. Binkley, R. Seeger, J. A. Pople, *J. Chem. Phys.* **1980**, *72*, 650-654.
- [5] M. Frisch, G. Trucks, H. Schlegel *et al*, Gaussian 09, Revision B.01, Gaussian, Inc., Wallingford CT, **2010**.
- [6] S. Yang, Y. Gong, J. Zhang, L. Zhan, L. Ma, Z. Fang, R. Vajtai, X. Wang, P. M. Ajayan, *Adv. Mater.* **2013**, *25*, 2452-2456.
- [7] H. Zhang, X. Lv, Y. Li, Y. Wang, J. Li, *ACS Nano* **2010**, *4*, 380-386.
- [8] P. A. Kilmartin, H. L. Zou, A. L. Waterhouse, *J. Agr. Food Chem.* **2001**, *49*, 1957-1965.
- [9] M. Ozyurek, N. Gungor, S. Baki, K. Guclu, R. Apak, *Anal. Chem.* **2012**, *84*, 8052-8059.